



4-to-1 Transimpedance combining amplifier-based static unitary detector for high-resolution of LADAR sensor

Eun-Gyu Lee¹ · Jae-Eun Lee¹ · Minhyup Song² · Gyu Dong Choi² · Bongki Mheen² · Bang Chul Jung¹ · Choul-Young Kim¹ 

Received: 18 May 2017 / Revised: 25 September 2017 / Accepted: 16 January 2018 / Published online: 25 January 2018
© Springer Science+Business Media, LLC, part of Springer Nature 2018

Abstract

A fully integrated 4-to-1 transimpedance combining amplifier (TICA)-based static unitary detector (STUD) is developed for high-resolution of laser detection and ranging (LADAR) sensor. With a developed TICA, the STUD is able to have an effective large-area photodetector to enlarge the region of interest (ROI) without the bandwidth deterioration of a receiver for LADAR sensor. The 4-to-1 TICA is fabricated using 0.18- μm standard CMOS technology and it consists of four independent current buffers, a two-stage signal combiner, a balun, an output buffer, and four over-current protectors in one single integrated chip. The core of the TICA dissipates a power of about 7.8 mW. The total power consumption, including that of the balun and the output buffer, is 41 mW from a 1.8-V supply. The average input-referred noise current spectral density is 15.4 pA/ $\sqrt{\text{Hz}}$ with a bandwidth of 185 MHz and a transimpedance gain of 70 dB Ω . The developed TICA occupies an active area of approximately 107 μm \times 102 μm and the die size, including the I/O pads, is 912 μm \times 1000 μm . From the two-dimensional optical pulse scanning measurements and the three-dimensional (3-D) range measurements, it is verified that the designed TICA is suitable for the receiver front-end of the STUD-based LADAR sensor.

Keywords Ladar receiver · Optical receiver · Readout IC (ROIC) · Static unitary detector · Transimpedance combining amplifier

1 Introduction

Laser detection and ranging (LADAR) sensors have been commonly used to acquire real-time three-dimensional (3-D) images using the time-of-flight (TOF) of a short laser pulse. Since a LADAR sensor has the potential to capture 3-D images of a fast-moving target, it has been deployed in many applications such as reconnaissance, autonomous vehicles and robots, remote sensing, terrain visualization, and surface mapping of buildings and scenes where high 3-D resolution is of prime importance [1–9]. For the acquisition of 3-D images the LADAR sensor must process

all the reflected TOF laser signals from every direction in the region of interest (ROI) in real-time. Currently, there are different operation methods for LADAR sensors with varying scanning mechanisms, number of lasers, and geometric configurations [10, 11].

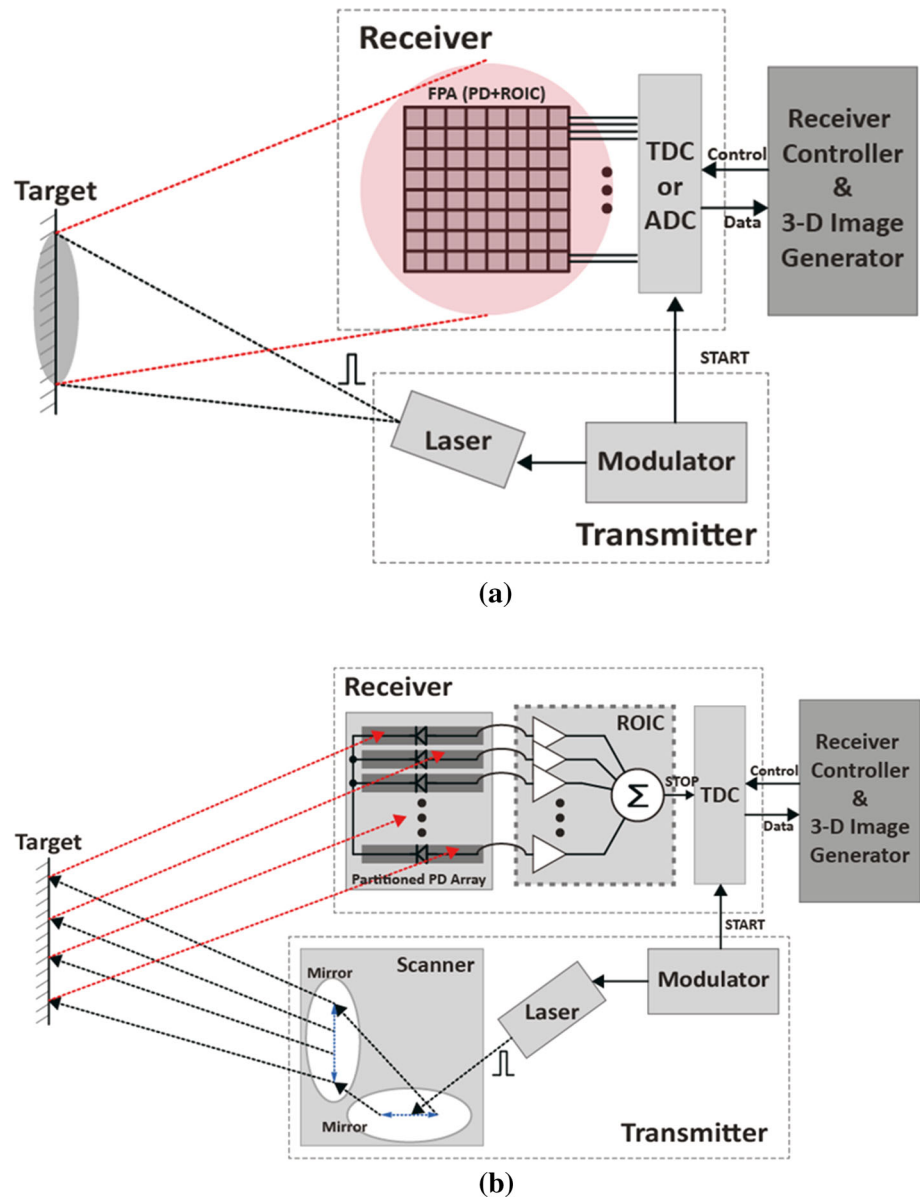
The FPA-based LADAR sensor [11] uses a two-dimensional array, a focal-plane array (FPA), of the photodetectors and a readout IC (ROIC) which is a similar method of obtaining a picture from the image sensor as shown in Fig. 1(a). This method provides an advantage in that it is possible to obtain a 3-D image of an object moving quickly without the need for a mechanical scanner. However, in order to obtain a high resolution 3-D image, the size of one pixel should be reduced to less than 100 μm , and the number of pixels in the FPA should be increased. Reducing the pixel size increases the interference between pixels, and minimizing cross talk between neighboring pixels requires spacing that results in poor resolution and sparse spatial sampling of the image [12].

✉ Choul-Young Kim
cykim@cnu.ac.kr

¹ Department of Electronics Engineering, Chungnam National University, Daejeon, South Korea

² Electronics and Telecommunication Research Institute, Daejeon, South Korea

Fig. 1 Block diagram. **a** FPA-based LADAR sensor. **b** STUD-based LADAR sensor



A new method, reported recently, is a static unitary detector (STUD)-based technique [13] as shown in Fig. 1(b). In the STUD-based LADAR sensor, two high-speed optical scanners for a transmitter and a large-area PD for a receiver are typically utilized. The transmitter illuminates one collimated pulse laser beam at a time in a specific direction over the entire ROI using two high-speed optical scanners. The receiver detects the returned optical pulses using a large-area static unitary PD, as illustrated in Fig. 2. The STUD-based LADAR receiver has multiple partitioned photosensitive cells to overcome bandwidth limitation caused by the large parasitic capacitance of the large-area photodetector. Each of the partitioned cells has its own transimpedance amplifier (TIA) to amplify the received signal in each cell independently, and a signal

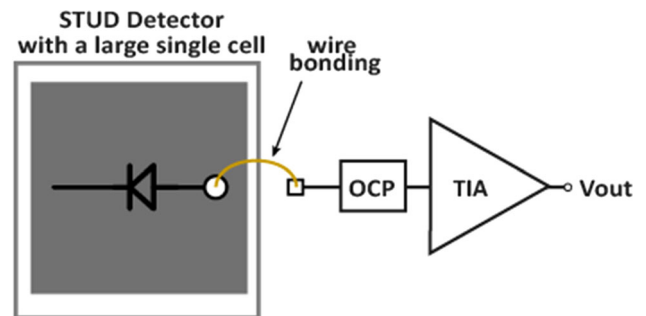


Fig. 2 Block diagram of receiver with a single large photodetector

combiner sums the outputs from all TIAs. The resolution of the 3-D image is determined by the two optical scanner in the STUD-based LADAR transmitter. According to [13],

the 3-D images with a very high resolution of 320 pixels \times 240 pixels were obtained with the STUD-based LADAR sensor.

However, to implement the STUD-based LADAR sensor, the number of TIAs required is the same as the number of partitioned photosensitive cells, and they are assembled on a single board. This restricts the number of cells for higher-resolution 3-D images for a large ROI, because of the interconnection problems between partitioned photodetectors and multiple TIAs [14]. To easily increase the effective photosensitive area for a large ROI, an ROIC designed for this specific purpose that is able to combine the optical currents from photosensitive cells into a single signal should be implemented. As a front-end readout circuit for the STUD-based LADAR receiver, the 4-to-1 transimpedance combining amplifier (TICA) is fully integrated on a single chip. With the fabricated TICA, it is possible to easily increase the effective photosensitive area of the STUD-based LADAR sensor. The TICA amplifies and combines the input photocurrents, converted from the incoming optical signals by the photosensitive cells, into a combined single voltage signal for further processing. It uses a two-input two-stage combining scheme considering a few parameters such as bandwidth, dynamic range, power consumption, noise and area. The 4-to-1 TICA is fabricated using the standard CMOS 0.18- μm technology. It provides an average input-referred noise current spectral density of 15.4 pA/ $\sqrt{\text{Hz}}$ with a bandwidth of 185 MHz and a transimpedance gain of 70 dB Ω . The core of the TICA consumes a power of approximately 7.8 mW, and the total power including the power consumptions of the balun and the output buffer is 41 mW from a 1.8-V supply. The core of the 4-to-1 TICA occupies an active area of approximately 107 μm \times 102 μm and the die size including the I/O pads is 912 μm \times 1000 μm .

The rest of this paper is organized as follows: in Sect. 2, the design specifications of the 4-to-1 TICA are described. Section 3 describes the detailed circuit architecture. In Sect. 4, the chip implementation and the experimental results are presented. Finally, the summary and conclusions are given in Sect. 5.

2 Design specifications of 4-to-1 TICA

In the optical receiver for the STUD-based LADAR sensor, the designed TICA is a front-end circuit directly connected to the photodetector, similar to the TIA. The difference is that the TICA has multiple input channels (the same number as the number of partitioned photosensitive cells) and it combines the input current signal into a single output voltage signal. Therefore, in the TICA design, the ability of signal summation should also be considered along with the

requirements of the TIA, such as the transimpedance gain, bandwidth, noise and stability. In particular, the minimum input current of the TICA needs to be estimated to set the goal for the transimpedance gain of the developed TICA.

The returned laser power is calculated using the LADAR range equation [15]. Assuming that, for an extended target, the footprint of the beam is smaller than the target surface, the returned power (P_r) can be calculated for Lambertian targets as follows:

$$P_r = P_t \cdot \rho \cdot \frac{D^2}{4R^2} \cdot \eta_{atm} \cdot \eta_{sys} \quad (1)$$

where P_t is the transmitted power, R is the travel distance of the laser beam, ρ is the reflectance of the target surface, and D is the aperture diameter of the receiver. η_{sys} and η_{atm} are the efficiency values of the optics of the system and the atmospheric attenuation, respectively [16].

The minimum detectable signal (MDS) of the STUD-based LADAR receiver is estimated using (1). Assuming that η_{sys} and η_{atm} are equal to 0.5, and the reflectivity of the target is 10–90%, for a lens diameter of 40 mm in the receiver and a laser peak power of 10 kW in the transmitter, the calculated returned power is approximately 2.5–22.5 μW for a maximum detectable range of 200 m. It corresponds to minimum input optical current of 15–135 μA with an assumed avalanche photo diode (APD) responsivity of 6 A/W. A minimum input current of 10 μA is targeted for the fabricated TICA to have sufficient margin for an object with low reflectivity and non-Lambertian reflection.

The level of the detected signal should rise above the noise level by an adequate margin to keep the detections caused by noise at a low level. A typical value in the pulsed measurements is a signal-to-noise ratio (SNR, which is the peak value of the current signal divided by the input-referred rms current noise) of 10 [8, 17]. As a result, the maximum input-referred rms current noise that can be detected reliably using the STUD-based LADAR is up to 1 μA with an above-minimum input current level of 10 μA . The noise of the receiver with multiple photosensitive cells increases since the noise from multiple photosensitive cells is summed in signal combining stage with an uncorrelated relation. Although input noise increases in the STUD-based receiver, the SNR is not degraded in the STUD-based LADAR receiver since input power level is notably higher than in other LADAR receivers.

In this work, the full width at half maximum (FWHM) of the input pulse is approximately 3.8 ns and its rise time is approximately 2 ns. The bandwidth required for the TICA to preserve its rise time can be approximated from [17] and [18] as:

$$BW \cong \frac{0.35}{t_r} \quad (2)$$

where t_r is the rise time of the input pulse. For a rise time of 2 ns, (2) gives a bandwidth of approximately 175 MHz. The bandwidth should not be designed to be wider than what is given by (2). It would only increase the receiver noise without decreasing the rise time of the laser [18]. An important feature of the STUD-based LADAR sensor is the partitioning of the photosensitive area of the APD into several cells. The APD used in this work has four photosensitive cells, as shown in Fig. 3. The size of each partitioned cell is $500 \mu\text{m} \times 140 \mu\text{m}$. The TICA is developed in the presence of a 2-pF photodiode parasitic capacitance (C_{PD}) for each partitioned cell.

In case a comparator is used next to the TICA for signal processing in the receiver, the comparator will have a minimum voltage level to determine the presence or absence of the signal. In addition, since the comparator generally has a hysteresis margin for noise immunity, the minimum input voltage level for the comparator would be approximately several tens of mV. This means that the minimum output voltage of the TICA should be of this level. In this work, the target for the minimum output voltage of the TICA is 30 mV for a minimum input current of 10 μA . Thus the transimpedance gain of the TICA must be larger than 70 dB- Ω .

For the STUD-based LADAR sensor, the design specifications for the 4-to-1 TICA with a 2-pF photodiode parasitic capacitance are summarized in Table 1.

3 Architecture description

The block diagram of the developed receiver with a 4-to-1 TICA is shown in Fig. 4. It amplifies and combines the photocurrents from the four partitioned photosensitive cells

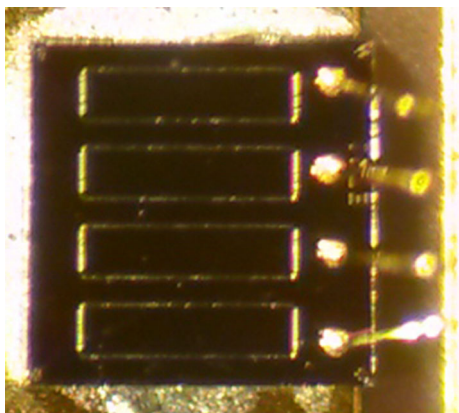


Fig. 3 Microphotograph of the photodetector partitioned into four photosensitive cells

Table 1 Summary of design specifications for 4-to-1 TICA

Parameter	Design target
Combining channel	4
Minimum detectable current (μA)	10
Maximum input-referred rms current noise (μA)	1
Bandwidth @ $C_{PD} = 2 \text{ pF}$ (MHz)	175
Transimpedance gain (dB Ω)	70

to one voltage signal. It is functionally equivalent to the block diagram in Fig. 2, but this scheme does not exhibit the bandwidth degradation caused by the large photodetector capacitance.

The 4-to-1 TICA consists of four over-current protection circuits (OCPs) that prevent the 4-to-1 TICA from being destroyed by a very large input signal, four current buffers acting as a low-impedance input stage to receive the optical current from each photodetector cell, and a signal combiner to sum the outputs of all current buffers. The signal combiner combines the signals from the four channels to a single signal through two stages. A post amplifier is designed as a bandwidth-enhancement stage.

The balun is a differential amplifier with differential input signals biased at the same DC level to convert the single-ended output of the signal combiner into a differential signal. A low-pass filter (LPF), for the DC coupling between the post amplifier and the balun, is added to induce the same DC voltages without additional DC bias. The output buffer is a differential amplifier, whose each output is matched to 50 Ω .

In Fig. 5, the schematic of the implemented receiver with 4-to-1 TICA is illustrated.

3.1 4-to-1 TICA

According to the working principle of the STUD-based LADAR sensor, the illuminated spot is changed with time in the ROI by the controlled optical scanner; thus, the position of the photons arriving at the photodetector changes. To reduce the bandwidth limitation caused by its large parasitic capacitance, the photodetector is partitioned into four photosensitive cells in this study, as shown in Fig. 3. The reflected photons may arrive at a single partitioned cell, or at two or more cells, according to the spot size of the arrived beam. Irrespective of when and where the returned signal arrives on the partitioned cells, it should be processed as a single signal. Therefore, in the STUD-based LADAR sensor with multiple photosensitive cells, the TICA is required to receive the photocurrent, similar to the TIA, and combine the input(s) into a single output without bandwidth degradation.

Fig. 4 Block diagram of designed receiver with a 4-to-1 TICA

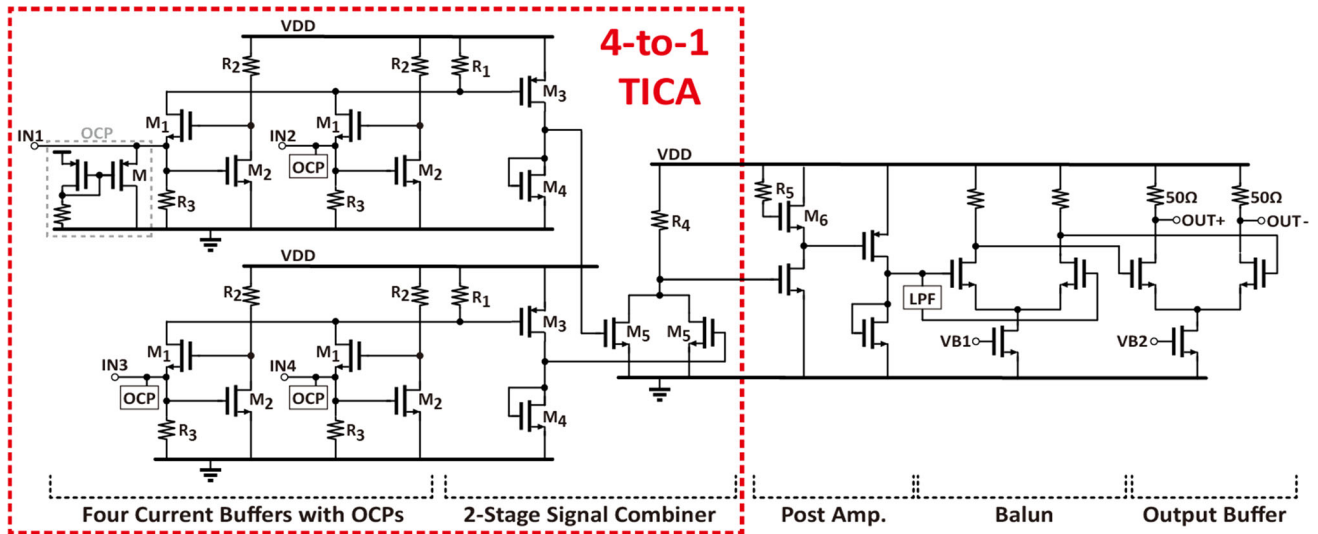
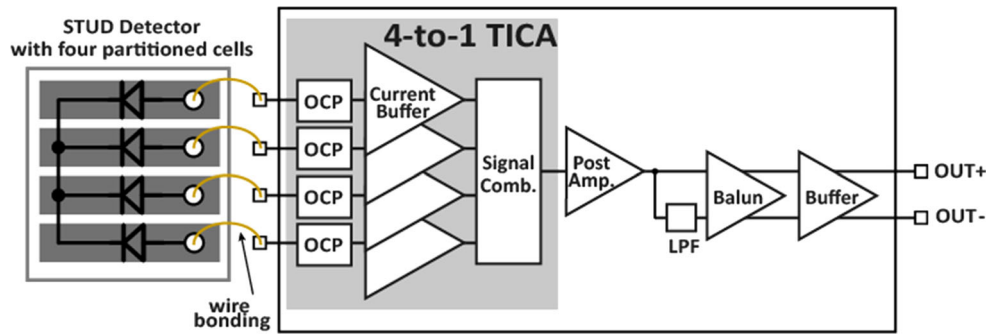


Fig. 5 Schematic of implemented receiver with 4-to-1 TICA

As shown in Fig. 5, the developed TICA has four copies of the regulated-cascode (RGC) topology as current buffers because of the low input impedance and wide bandwidth of the RGC topology, compared with the inverter, common-source, and common-gate topologies [19]. The RGC structure is used to release the input parasitic effects by reducing the input impedance significantly because of the M2 and R2 stages, which operate as a local feedback to boost the transconductance of M1. The small-signal input impedance of the RGC structure (Z_{in}) is given by (3):

$$Z_{in} \cong \frac{1}{g_{m1}(1 + g_{m2}R_2)} \quad (3)$$

where g_{m1} and g_{m2} are the transconductance of M1 and M2, respectively.

The simplest choice would be to combine all the signals, which means four signals in this work, in the first combining stage, as shown in Fig. 6. In this case, the bias current of each RGC current buffer should be reduced by the number of combined inputs N to retain proper DC bias voltages at the TIA outputs with a suitable transimpedance gain-defining resistor, R1 [19]. When the resistance of R1

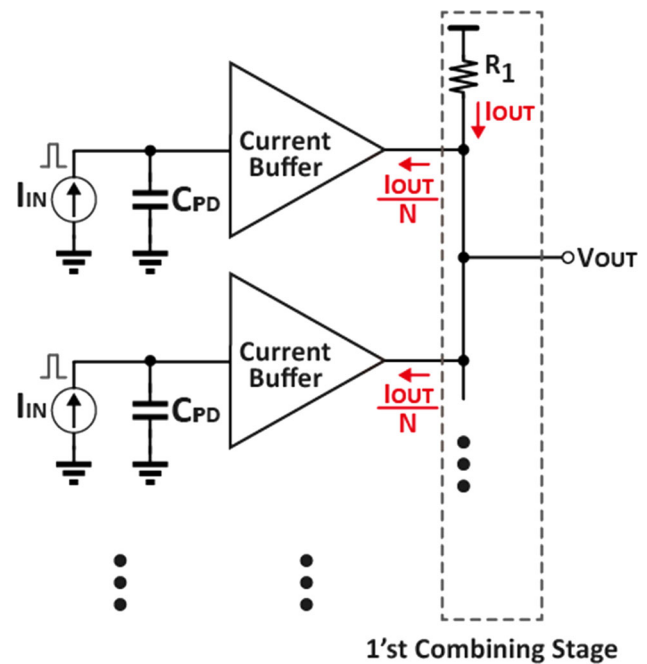


Fig. 6 Signal combining in the first stage

is set to the gain of the first stage by (4), and the DC bias voltage V_{OUT} is also set to the bias voltage of the next stage, the DC bias current of I_{OUT} is calculated to a specific value. Therefore, increasing the number of combined inputs N causes a decrease in the DC current for the input current buffer stage by N .

$$Z_{T,RGC} \cong R_1 \tag{4}$$

However, reducing the bias current limit the maximum current that can be detected without saturation at the receiver input stage, which means that the dynamic range of the receiver is decreased. Figure 7 represents the simulated output peak voltages as functions of the input current and the number of combining inputs N in the first combining stage. It can be seen from Fig. 7 that the maximum detectable current of the input current buffer stage decreases as N increases. Table 2 shows the performance comparison of some parameters according to N . With similar transimpedance gains, as N decreases, the bandwidth and the input-referred noise current density improves; however, it requires larger static currents and area for implementing the additional combining stages. The case of $N = 3$ is not suitable for combining four inputs. In case of $N = 1$, the proposed scheme combining the signals in the RGC TIA stage cannot be used. On comparing the cases of $N = 2$ and $N = 4$, it can be observed that $N = 2$ has better performances in dynamic range, bandwidth and noise; however, it consumes more power because of the additional combining stage. Even though the timing mark does not depend on the detected input amplitude, the dynamic range for LADAR receiving using the leading-edge timing discrimination is important for walk error compensation since the input current amplitude has wide variation according to the detection range and reflectivity of the target object. Therefore, we choose $N = 2$ for the 4-to-1 TICA with a wider dynamic

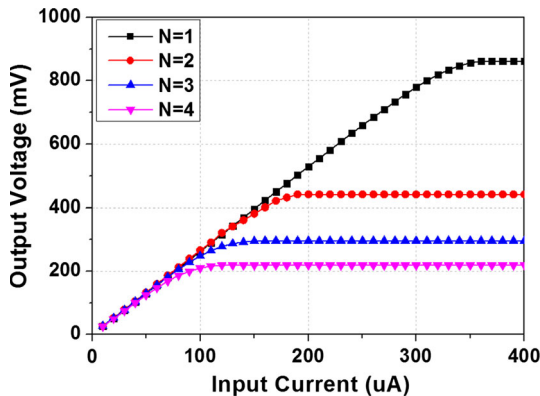


Fig. 7 Simulated dynamic range of the RGC input stage according to the number of combining inputs

range, and the TICA is designed using the two-input two-step combining topology.

The gain of the 4-to-1 TICA for a single signal path can be simplified as:

$$Z_{T,TICA}(0) \cong Z_{T,RGC}(0) \cdot A_{v,C2}(0) = R_1 \cdot g_{m3}BR_4 \tag{5}$$

where $A_{v,C2}$ is the voltage gain of the second combining stage, g_{m3} is the transconductance of transistor M_3 , and B is the size ratio of transistor M_4 to M_5 .

The -3 -dB bandwidth of the TICA is given by (6):

$$f_{-3\text{ dB}} \cong \frac{1}{2\pi \frac{C_{in,total}}{g_{m1}(1+g_{m2}R_2)}} \tag{6}$$

where $C_{in,total}$ is the total input capacitance of the TICA that is given by $C_{in,total} \approx C_{PD} + C_{gs2} + C_{sb1}$.

To analyze the effect of the noise introduced by partitioned photosensitive cells and the TICA, the simplified circuit is illustrated in Fig. 8 while equivalent noise sources are considered. The equivalent total input referred noise of the TICA is approximately given by (7)

$$\begin{aligned} \overline{i_{n,in}^2} &\cong \frac{\overline{v_{n,OUT}^2}}{Z_{T,TICA}} \\ &= \left\{ 4 \left(\overline{i_{n,PD}^2} + \overline{i_{n,CB}^2} \right) + 2\overline{i_{n,R1}^2} \right\} \cdot R_1 \\ &\quad + \frac{\left(2\overline{i_{n,C2}^2} + \overline{i_{n,R4}^2} \right) \cdot R_4^2}{Z_{T,TICA}} \end{aligned} \tag{7}$$

where $\overline{i_{n,PD}^2}$ is the noise from a single photosensitive cell, $\overline{i_{n,CB}^2}$ is the generated noise in the current buffer stage, $\overline{i_{n,C2}^2}$ is the generated noise in the second combining stage, and $\overline{i_{n,R1}^2}$ and $\overline{i_{n,R4}^2}$ are the thermal noise from R_1 and R_4 , respectively. In this analysis, we assume that,

$$\overline{i_{n,PD}^2} = \overline{i_{n,PD1}^2} = \overline{i_{n,PD2}^2} = \overline{i_{n,PD3}^2} = \overline{i_{n,PD4}^2}$$

$$\overline{i_{n,CB}^2} = \overline{i_{n,CB1}^2} = \overline{i_{n,CB2}^2} = \overline{i_{n,CB3}^2} = \overline{i_{n,CB4}^2}$$

$$\overline{v_{n,C1}^2} = \overline{v_{n,C1,1}^2} = \overline{v_{n,C2,2}^2}$$

$$\overline{i_{n,C2}^2} = \overline{i_{n,C2,1}^2} = \overline{i_{n,C2,2}^2}$$

In (7), the receiver noise with a large-area photodetector, even though it is partitioned, is increased in the developed TICA. The noise generated in the first combining stage with the current buffer is also the dominant factor of the equivalent total noise. As mentioned earlier, the permitted noise level of the STUD-based LADAR receiver is notably higher than that of the FPA-based LADAR receiver. However, further optimization in the combining circuit is necessary to improve the sensitivity.

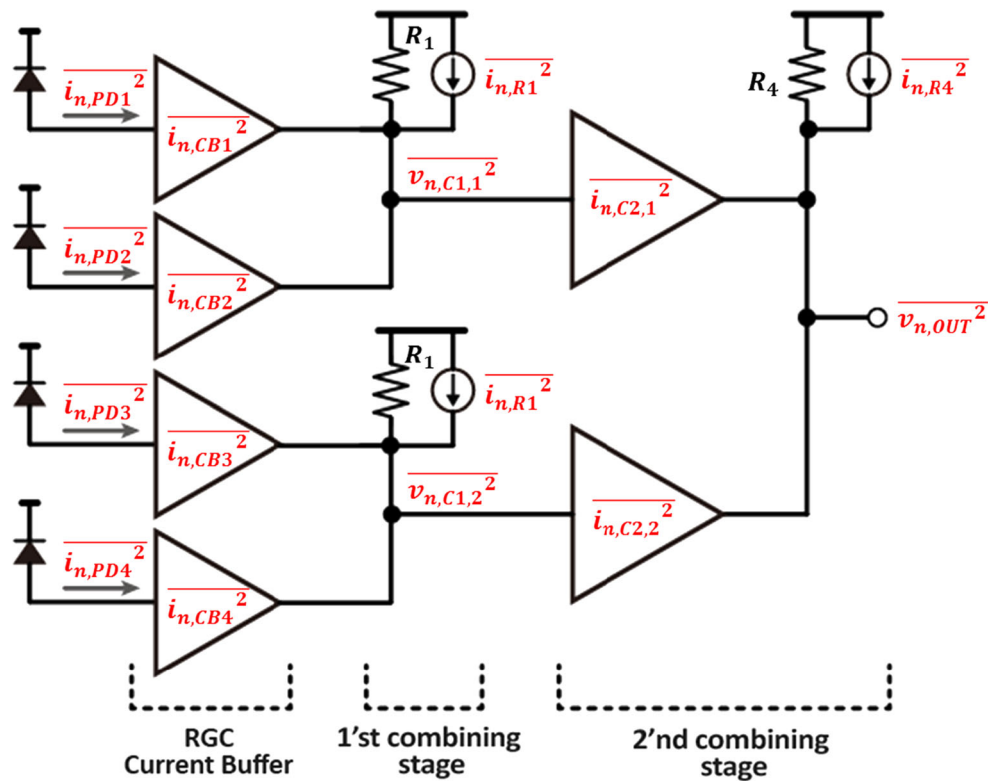
The post amplifier is designed with a two-stage common-source amplifier. The first stage has an active inductor

Table 2 Performance comparison according to the number of combining inputs N

	$N = 1$	$N = 2$	$N = 3$	$N = 4$
Transimpedance gain (dBΩ)	68.22	68.56	68.68	68.74
Bandwidth (MHz)	368	280	227	193
Input-referred noise current density (pA/√Hz)	7.4	7.6	7.7	8.0
DC current (mA)	0.50	0.83 (2.81*)	1.16	1.51
Suitable structure	X	O	X	O

*Total current of two-input two-stage combining circuit

Fig. 8 Simplified circuit for noise analysis



load consisting of a transistor M6 and a resistor R5 [20] to enhance the overall bandwidth, and the second stage is for the pulse polarity and DC bias.

The over-current protection circuit, as shown in Fig. 5, is designed to protect the 4-to-1 TICA from being damaged by a very high input photocurrent [21]. The transistor M turns on only when its source voltage is larger than 1.1 V, and M is large enough to sink several mA. When the input current is approximately 600 μA, the source voltage of M reaches 1.1 V.

3.2 Balun and output buffer

The balun is designed to convert the single-ended TICA output signal to differential signals. The balun is a differential amplifier with differential inputs biased at the same DC level. In this work, an LPF is inserted for the DC coupling between the combining stage and the input of the

balun to provide the required DC level, as shown in Fig. 5. One input of the balun receives the pulse signal with its own DC bias, which is set from the first stage, and the DC coupling with the LPF induces the same DC voltage at the other input of the balun. The implemented LPF occupies an area of 75 μm × 30 μm, and additional DC bias is not required for the balun. The output buffer, as shown in Fig. 5, is also a differential amplifier and it is designed to match the output impedances to 50 Ω. With this balun and output buffer, the simulated transimpedance gain of the developed TICA is depicted in Fig. 9. The transimpedance gain is approximately 70 dBΩ and the - 3 dB frequency is approximately 185 MHz with a photodetector parasitic capacitance of 2 pF. The bandwidth must be high enough to preserve the shape of the laser pulse but should not be wider than the value given by (2) in the aspect of receiver noise [8].

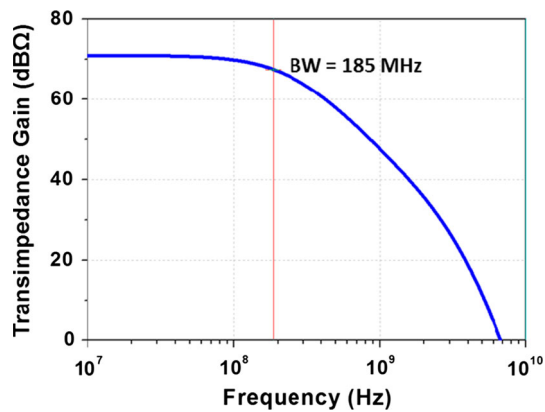
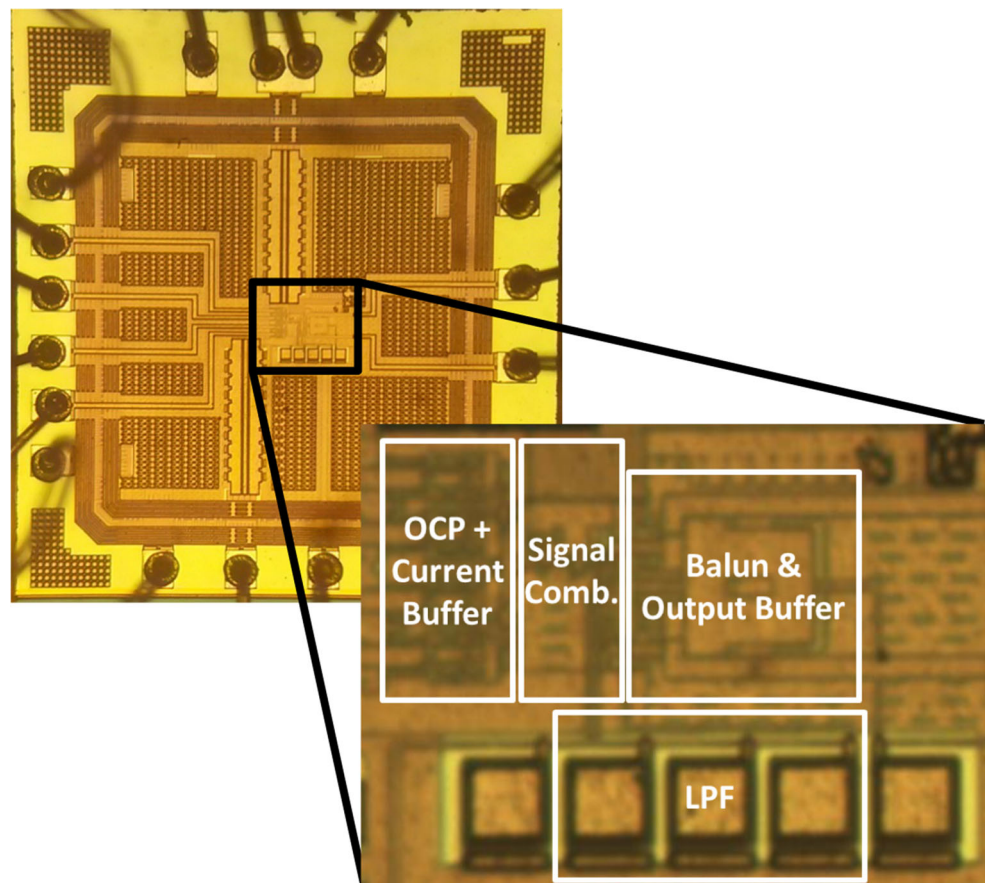


Fig. 9 Simulated transimpedance gain of the designed circuit

4 Measurement results

The receiver with the TICA was fabricated using the CMOS 0.18- μm process, and a microphotograph of the chip is shown in Fig. 10. The total chip size, including the I/O pads, is $912\ \mu\text{m} \times 1000\ \mu\text{m}$, and the core circuit occupies an area of $107\ \mu\text{m} \times 102\ \mu\text{m}$. All the biases were applied through bond wires, and short pulse response measurements were performed using a CMJ connector.

Fig. 10 Chip microphotograph of the fabricated receiver with 4-to-1 TICA chip



For facilitating the electrical pulse response measurements, the fabricated chip was mounted on a wire-bonded chip-on-board (COB) module, as shown in Fig. 11(a). A 10-k Ω resistor acts as a voltage-to-current converter. To measure the transient response of the fabricated circuit, an electrical pulse signal generated from an Agilent 81110A pattern generator was applied to each input channel of the implemented test fixture as shown in Fig. 11(b). The OUT1 and OUT2 signals were measured using an Agilent DSO7104B oscilloscope.

Figure 12 shows the simulated and measured transient pulse responses for the fabricated chip. The pulse magnitude of the input voltage from the pattern generator is adjusted so that the input current is 20 μA and the pulse width of the input signal is 3.8 ns with a rise time of 2 ns. The measured output pulses are almost the same and show a good correspondence with the simulated results. The transimpedance gain is calculated as approximately 70 dB Ω . Figure 13 shows the dependence of the 4-to-1 TICA output voltage amplitude on the input current. The output voltage swing is linear for input current variations up to 60 μA with the maximum output voltage swing of approximately 200 mV for both OUT+ and OUT-. This

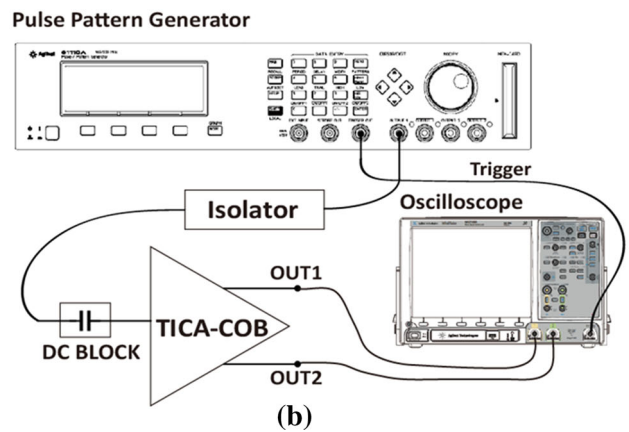
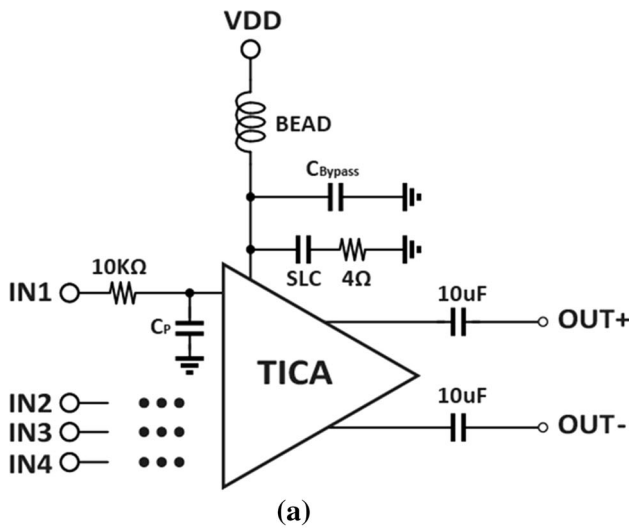


Fig. 11 a TICA-COB schematic for electrical pulse response. b Measurement setup for electrical pulse response

measured result matches well with the simulated results, shown by the dotted curve in Fig. 13.

The frequency response of the implemented TICA is measured by S21, as shown in Fig. 14. The S21 is measured from 10 MHz to 400 MHz using an Agilent N5224A. The measured -3 dB bandwidth is approximately 220 MHz which is 35 MHz larger than the simulated bandwidth of 185 MHz.

The integrated single-ended output noise of the 4-to-1 TICA was measured via the oscilloscope RMS calculation function with no input signal source, as shown in Fig. 15 [22]. The standard deviation of the output was measured to be 1.417 mV. After subtracting the inherent oscilloscope noise of 0.4 mV_{rms}, the corrected single-ended integrated output noise of the TICA was estimated at 1.359 mV_{rms}. The integrated input-referred noise of the differential output of the 4-to-1 TICA for each input can be calculated as [23]:

$$I_{n,in} = \frac{1}{4} \cdot \frac{2\sqrt{(1.417 \text{ mV})^2 - (0.4 \text{ mV})^2}}{70 \text{ dB}\Omega} = 0.21 \mu\text{A}_{rms} \tag{8}$$

The average input-referred noise current density is

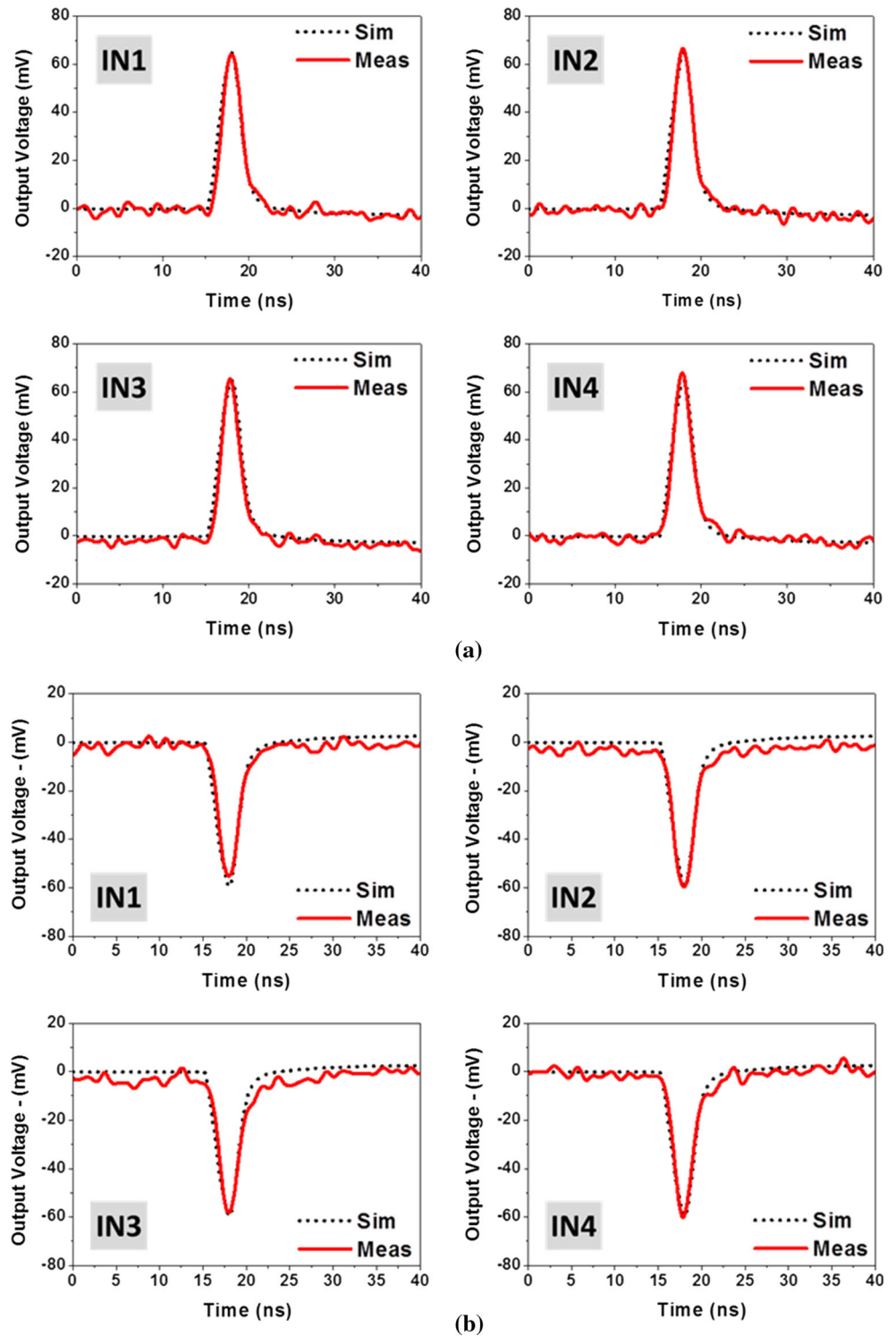
$$I_{n,in,avg} = \frac{I_{n,in}}{\sqrt{BW}} = 15.4 \text{ pA}/\sqrt{\text{Hz}} \tag{9}$$

The 4-to-1 TICA used a supply voltage of 1.8 V and dissipated 41 mW of power, including the core consumption of 7.8 mW. The performances of the TICA are summarized in Table 3. These results almost meet the requirements in Table 1. Table 3 additionally shows a comparison between the implemented TICA and the other TIAs. These results demonstrate that the designed TICA performs the conversion of the photocurrent to the voltage signal as well as the general TIAs, and is also suitable as the front-end circuit for an effectively large area photodetector with parasitic capacitance of 8 pF through the signal combining method.

Additionally, the two-dimensional (2-D) optical pulse scanning measurement was performed using the test fixture in Fig. 16(a). In the test fixture, the four partitioned cells and the fabricated TICA were mounted on a wire-bonded COB module. The size of a single photosensitive cell was 500 μm × 140 μm. The measurement was carried out using a laser pulser with a peak output power of 6.7 W, wavelength of 1550 nm, FWHM of 3.8 ns, and repetition rate of 120 kHz. This laser pulse was used to illuminate the partitioned APD through an attenuator, collimator, and receiving optics. The position of the illuminated spot on the APD was changed in time by the two stepper motors. The 2-D mechanical scanning was implemented with two stepper motors in two directions (X and Y). The peak-to-peak output voltage from the fabricated chip was measured by an oscilloscope, as shown in Fig. 16(b).

In the given experimental setup, the 2-D output voltages were collected from a 1000 μm × 1000 μm area according to the spot size of the focused beam. First, to verify that the four input paths are operated independently, the 2-D scan measurements were carried out at the point in focus. In this case, the beam spot size that arrived at the optical test fixture was smaller than the space between the cells. Figure 17(a) shows the 2-D scanned intensity image and its normalized 3-D intensity mesh image with a scan resolution of 10 μm × 10 μm at that position. There are four partitioned photosensitive areas, which represent the photodetector in Fig. 3. The horizontal length of a single photosensitive area, calculated at a 50% threshold of the output amplitude in Fig. 17(a), is approximately 520 μm, and is comparable to the known value. From this result, it is possible to confirm that the 4-to-1 TICA is operated

Fig. 12 Simulated and measured pulse response at 20 μA input pulse. **a** OUT1. **b** OUT2



independently even if the input current is applied to any single input path. However, in the LADAR receiver, if the reflected pulse arrives in the area between the cells, the range information cannot be obtained. To overcome this problem, the beam spot size on the photodetector should be larger than the space between the photosensitive cells so

that the arriving photons can be spread over two or more cells. This can be easily accomplished by adjusting the focus. Figure 17(b) shows the results with a scan resolution of $20\ \mu\text{m} \times 20\ \mu\text{m}$ at a position behind the focal point. This makes the beam spot size on the photodetector larger, and then, four partitioned cells seem like a large single

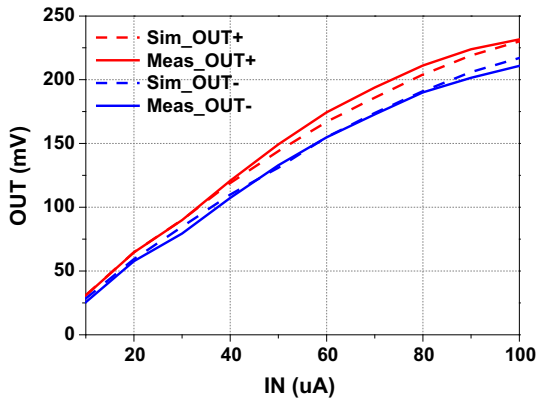


Fig. 13 Simulated and measured output voltage amplitude versus input current at differential output

photodetector without any blind area, as shown in Fig. 17(b). It means that there is no signal loss even if the photodetector is separated, since the signal-combining function of the fabricated TICA has worked properly when the beam spot size on the photodetector was large enough to cover several cells.

Fig. 14 Simulated and measured transimpedance frequency response

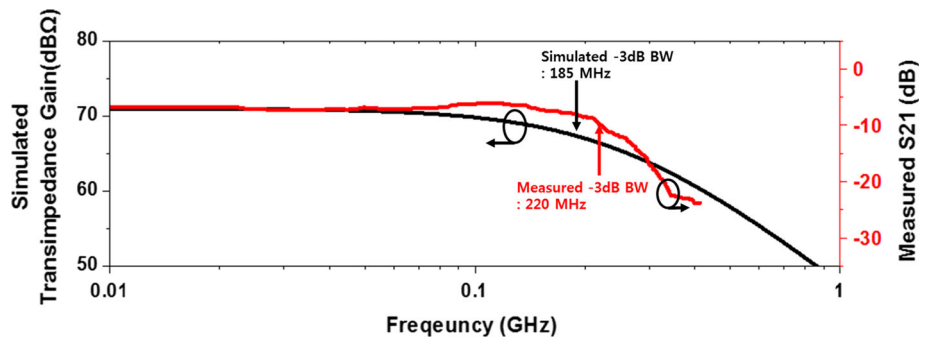
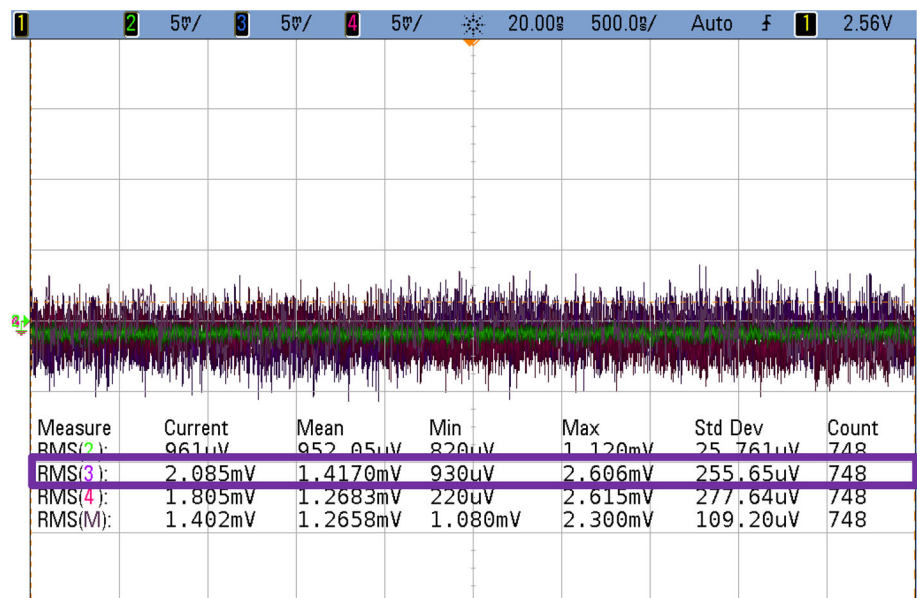


Fig. 15 Measured single-ended integrated output noise of the TICA



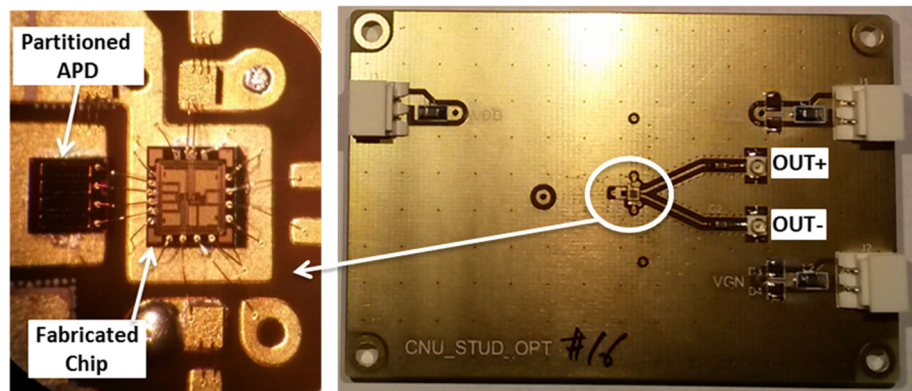
The intensity and 3-D range images for a remote object—a book-end—obtained from the STUD-based LADAR sensor using the developed receiver with the 4-to-1 TICA are shown in Fig. 18(a). The fabricated TICA was set behind optics in the STUD-based LADAR receiver. The transmitter illuminated laser pulses with two scanners, and then the receiver measured the intensity and range from the reflected pulse and captured the images. In some holes of the book-end image, there is additional range information about another object behind the book-end. The simplified experimental environment is illustrated in Fig. 18(b).

These results prove that the fabricated 4-to-1 TICA worked well in the STUD-based high-resolution 3-D LADAR receiver and the photosensitive area is effectively increased with the TICA.

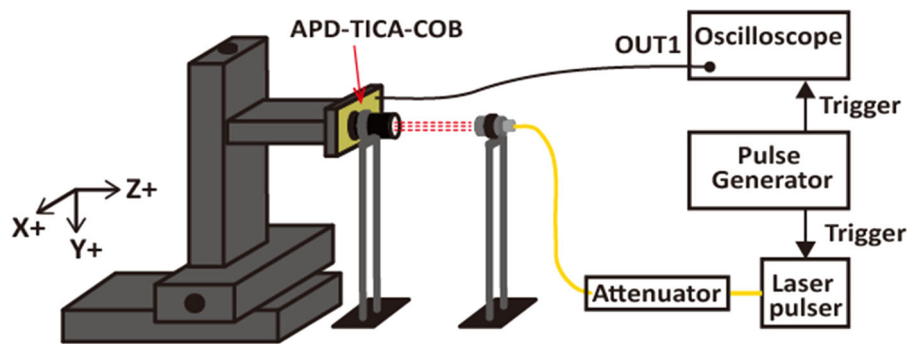
Table 3 Summary of 4-to-1 TICA performances

Parameter	This work	[8]	[21]	[24]	[25]*
Combining channel	4	NA	NA	NA	NA
C_{PD} (pF)	2×4 cells	1.5	2	2.5–5	2
Transimpedance gain (dB Ω)	70	81	78	80	87
Bandwidth (MHz)	185*	230	640	160	150
Input-referred rms noise (μ A)	0.21	0.05	0.12	0.02	0.10
Power consumption (mW)	41	115	114	79	165
Chip size (mm ²)	0.9×1.0	1.85×1.85	0.89×0.66	1.2×1.2	NA
Technology (μ m)	CMOS 0.18	BiCMOS 0.35	CMOS 0.13	CMOS 0.35	CMOS 0.18

*Simulation results

Fig. 16 **a** Photograph of APD-TICA-COB (optical test fixture). **b** Measurement setup for 2-D optical pulse response

(a)



(b)

5 Conclusion

The STUD-based LADAR sensor with a compact fully integrated 4-to-1 TICA was presented for high-resolution 3-D image acquisition over a large ROI. Since the chip size of TICA, which integrates multiple TIAs and signal combiners on a single chip, is similar to the size of an APD, the connection between the two devices could be applied through bond wires at distances of several hundred micrometers. The fabricated chip had a 41-mW power consumption with a core consumption of 7.8 mW at 1.8-V

supplied voltage, an average input-referred noise current spectral density of $15.4 \text{ pA}/\sqrt{\text{Hz}}$, and a transimpedance gain of 70 dB Ω . The chip was operated based on the same working principle as the STUD-based LADAR receiver, and a 3-D range image was obtained by using the developed receiver with the TICA. As one integrated chip, the developed TICA is suitable for the STUD-based LADAR sensor used for high-resolution 3-D image acquisition over a large ROI that can be applied in unmanned vehicles, automobiles, surveillance, etc.

Fig. 17 **a** In-focus measured intensity image from 2-D scan. **b** Defocused intensity image from 2-D scan

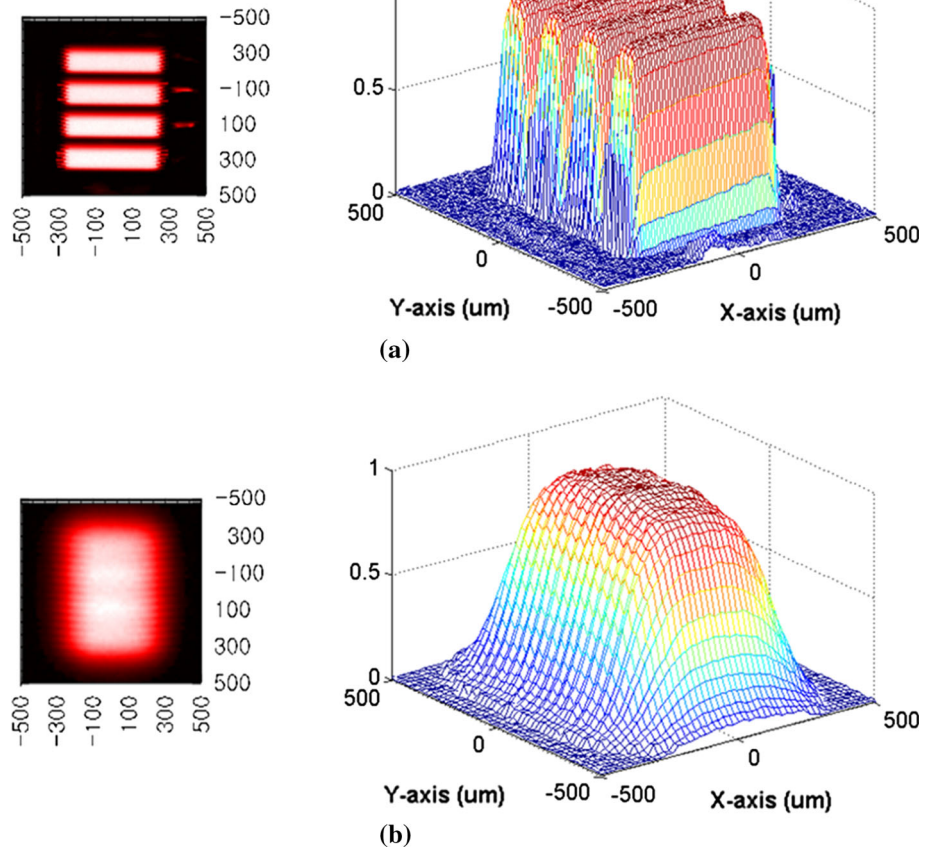
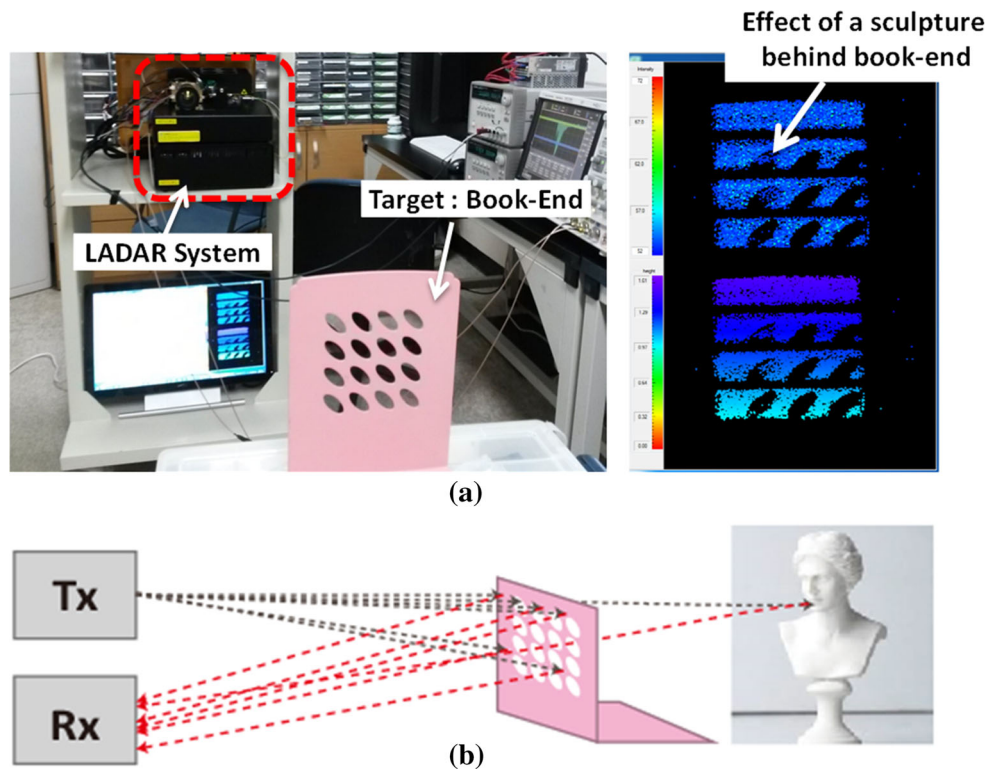


Fig. 18 **a** Measured 3-D range image. **b** The simplified experimental environment



Acknowledgements This research was supported in part by Basic Science Research Program through the National Research Foundation of Korea (NRF) funded by the Ministry of Science and ICT (NRF-2015R1C1A1A01052508) and in part by Basic Science Research Program through the NRF funded by the Ministry of Science and ICT (NRF-2016R1A2B4014834).

References

- Thrun, S., Montemerlo, M., Dahlkamp, H., Stavens, D., Aron, A., Diebel, J., et al. (2006). Stanley: The robot that won the DARPA grand challenge. *Journal of Field Robotics*, 23(9), 661–692.
- Kaisto, I., Kostamovaara, J., Moring, I., & Myllyla, R. (1990). Laser rangefinding techniques in sensing of 3-D objects. In *Proc. SPIE*, Santa Clara, CA, vol. 1260, pp. 122–133.
- Larsson, U., Forsberg, J., & Wernersson, Å. (1996). Mobile robot localization: Integrating measurements from a time-of-flight laser. *IEEE Transactions on Industrial Electronics*, 43(3), 422–431.
- Chung, W., Kim, S., Choi, M., Choi, J., Kim, H., Bae Moon, C., et al. (2009). Safe navigation of a mobile robot considering visibility of environment. *IEEE Transactions on Industrial Electronics*, 56(10), 3941–3949.
- Wang, C., & Glenn, N. F. (2009). Integrating LIDAR intensity and elevation data for terrain characterization in a forested area. *IEEE Geoscience and Remote Sensing Letters*, 6(3), 463–466.
- Amzajerjian, F., Gao, C.-Q., & Xie, T.-Y. (2009). 3D imaging LADAR with linear array devices: laser, detector and ROIC. In *Proc. SPIE*, vol. 7382, p. 738209.
- Li, T.-H. S., Yeh, Y.-C., Wu, J.-D., Hsiao, M.-Y., & Chen, C.-Y. (2010). Multifunctional intelligent autonomous parking controllers for carlike mobile robots. *IEEE Transactions on Industrial Electronics*, 57(5), 1687–1700.
- Kurtti, S., & Kostamovaara, J. (2011). An integrated laser radar receiver channel utilizing a time-domain walk error compensation scheme. *IEEE Transactions on Instrumentation and Measurement*, 60(1), 146–157.
- Fersch, T., Weigel, R., & Koelpin, A. (2017). A CDMA modulation technique for automotive time-of-flight LiDAR systems. *IEEE Sensors Journal*. <https://doi.org/10.1109/JSEN.2017.2688126>.
- Glennie, C., & Lichti, D. D. (2010). Static calibration and analysis of the velodyne HDL-64E S2 for high accuracy mobile scanning. *Remote Sensing*, 2, 1610–1624.
- Stettner, R., Bailey, H., & Silverman, S. (2008). Three dimensional Flash LADAR focal planes and time dependent imaging. *International Journal of High Speed Electronics and Systems*, 18(2), 401–406.
- Shrekenhamer, D., Xu, W., Venkatesh, S., Schurig, D., Sonkusale, S., & Padilla, W. J. (2012). Experimental realization of a metamaterial detector focal plane array. *Physical Review Letters*, 109(17), 177401.
- Mheen, B., Shim, J.-S., Oh, M. S., Song, J., Song, M., Choi, G. D., et al. (2014). High-resolution three-dimensional laser radar with static unitary detector. *Electronics Letters*, 50(4), 313–315.
- Lee, E.-G., An, J., & Kim, C.-Y. (2014). A fully integrated four-input combining receiver front-end circuit for laser radar with static unitary detector. *Electronics Letters*, 50(21), 1543–1545.
- Richmond, R. D., & Cain, S. C. (2010). *Direct-detection LADAR systems*. Bellingham: SPIE Press. <https://doi.org/10.1117/3.836466>.
- Kim, S., Lee, I., & Kwon, Y. J. (2013). Simulation of a Geiger-mode imaging lidar system for performance assessment. *Sensors*, 2013(13), 8461–8489.
- Ziemer, R., & Tranter, W. (1985). *Principles of communications* (2nd ed.). Boston, MA: Houghton Mifflin.
- Ruotsalainen, T., Palojarvi, P., & Kostamovaara, J. (2001). A wide dynamic range receiver channel for a pulsed time-of-flight laser radar. *IEEE Journal of Solid-State Circuits*, 36(8), 1228–1238.
- Park, S. M., & Yoo, H. (2004). 1.25-Gb/s regulated cascode CMOS transimpedance amplifier for gigabit ethernet applications. *IEEE Journal of Solid-State Circuits*, 39(1), 112–121.
- Lee, T. H. (2003). *The design of CMOS radio-frequency integrated circuits* (2nd ed.). Cambridge: Cambridge University Press.
- Ngo, T.-H., Kim, C.-H., Kwon, Y. J., Ko, J. S., Kim, D.-B., & Park, H.-H. (2013). Wideband receiver for a three-dimensional ranging LADAR system. *IEEE Transactions on Circuits and Systems I: Regular Papers*, 60(2), 448–456.
- Weiner, J. S., Lee, J. S., Leven, A., Baeyens, Y., Houtsma, V., Georgiou, G., et al. (2004). An InGaAs-InP HBT differential transimpedance amplifier with 47-GHz bandwidth. *IEEE Journal of Solid-State Circuits*, 39(10), 1720–1723.
- Li, C., & Palermo, S. (2013). A low-power 26-GHz transformer-based regulated cascode SiGe BiCMOS transimpedance amplifier. *IEEE Journal of Solid-State Circuits*, 48(5), 1264–1275.
- Cho, H.-S., Kim, C.-H., & Lee, S.-G. (2014). A high-sensitivity and low-walk error LADAR receiver for military application. *IEEE Transactions on Circuits and Systems I: Regular Papers*, 61(10), 3007–3015.
- Zheng, H., Ma, R., & Zhu, Z. (2017). A linear and wide dynamic range transimpedance amplifier with adaptive gain control technique. *Analog Integrated Circuits and Signal Processing*, 90(1), 217–226.



Eun-Gyu Lee received the B.S. degree in electronics engineering from Chungnam National University (CNU), Daejeon, Korea, in 2004 and M.S. degrees in electrical engineering from Pohang University of Science and Technology (Postech), Pohang, Korea, in 2006. She is working on her Ph.D. degree in electronics engineering in CNU. Her research interests include readout integrated circuits and systems for laser radar applications.



Jae-Eun Lee received the B.S. degree in electronics engineering from Chungnam National University (CNU), Daejeon, Korea, in 2006. He is working on his M.S. degree in electronics engineering in CNU. His research interests include readout integrated circuits and systems for laser radar applications.



Minhyup Song received his B.S. degree in electrical engineering from the Korea University, Seoul, Korea, in 2006, and the direct Ph.D. degree in electrical engineering from Purdue University, West Lafayette, IN, USA, in 2012. From 2009 to 2012, he was a Research Assistant with the Ultrafast Optics and Optical Fiber Communications Laboratory. He was engaged in research on microwave photonic filter design based on optical frequency

comb source, where his research result was highlighted by Nature Photonics. In 2013, he joined the components and material research laboratory in Electronics and Telecommunication Research Institute (ETRI) as a senior researcher, where he is currently working on three-dimensional LADAR image sensor for autonomous vehicles. Dr. Song is a member of the Optical Society of America and IEEE. He has served as a reviewer for Journal of Optics Letter, Optics Express, IEEE Photonic Technology Letters, and Journal of the Optical Society of America B. He is the author of more than 15 articles, and is the inventor of 8 U.S. patents. His awards include the Marquis Who's who in America in 2015 and 2016, and Marquis Who's who in the world in 2016.



Gyu Dong Choi received the B.S. degrees in computer science and electronics from the Chonbuk National University, in 2008 and the M.S. degree in information and communications from Gwangju Institute of Science and Technology, Gwangju, Republic of Korea, in 2010. From 2010 to 2013, he studied Neuroscience in the Implantable Microsystems Laboratory, Gwangju Institute of Science and Technology. Since 2013, he has been a Researcher

with the Photonic/Wireless Convergence Components Research Department, Electronics and Telecommunications Research Institute. His research interests include signal processing and improvement of the SNR of laser radar system and high efficiency scanning method for LADAR system and applications.



Bongki Mheen received the M.S. degree in electrical and electronic engineering from Pohang University of Science and Technology (POSTECH), Gyungbuk, Korea, in 2000, and the Ph.D. degree in electrical engineering from Korea Advanced Institute of Science and Technology (KAIST), Daejeon, Korea, in 2006. Since 2000, he has been with the Electronics and Telecommunication Research Institute (ETRI), Korea, and has been

engaged in the research and development of silicon/compound based

device optimization, and circuit and system design, including high-performance SiGe HBT and strained MOSFET, $1/f$ noise analysis, broadband silicon photonics, low-noise CMOS image sensor, and system design for RADAR and LIDAR applications. From 2007 to 2008, he was also a Postdoctoral Research Fellow at Delft University of Technology (TU Delft), Netherlands. Dr. Mheen is a project leader of the patented Static Unitary Detector (STUD) LIDAR technology which showed world-best high-performance real-time 3D images. His research interests are mainly focused on a low-cost and high-performance three-dimensional LIDAR for autonomous vehicles utilizing both of silicon and compound technology.



Bang Chul Jung received the B.S. degree in electronics engineering from Aju University, Suwon, South Korea, in 2002, and the M.S. and Ph.D. degrees in electrical and computer engineering from Korea Advanced Institute of Science and Technology (KAIST), Daejeon, South Korea, in 2004 and 2008, respectively. He was a Senior Researcher/Research Professor with KAIST Institute for Information Technology Convergence, Daejeon, South

Korea, from 2009 to 2010. From 2010 to 2015, he was a Faculty member with Gyeongsang National University. He is currently an Associate Professor of the Department of Electronics Engineering, Chungnam National University, Daejeon, South Korea. His research interests include 5G mobile communication systems, statistical signal processing, opportunistic communications, compressed sensing, interference management, interference alignment, random access, relaying techniques, device-to-device networks, in-network computation, and network coding. Dr. Jung was a recipient of the Fifth IEEE Communication Society Asia-Pacific Outstanding Young Researcher Award in 2011. He also received the Haedong Young Scholar Award in 2015, which is sponsored by the Haedong Foundation and given by Korea Institute of Communications and Information Science.



Choul-Young Kim received his B.S. degree in electrical engineering from Chungnam National University, Daejeon, Rep. of Korea, in 2002 and his M.S. and Ph.D. degrees in electrical engineering from the Korea Advanced Institute of Science and Technology, Daejeon, Rep. of Korea, in 2004 and 2008, respectively. From March 2009 to February 2011, he was a postdoctoral research fellow at the Department of Electrical and Computer Engineering, University of California, San Diego, USA. Currently, he is working an

assistant professor of electronics engineering at Chungnam National University. His research interests include RF/mm-wave integrated circuits and systems for short-range radar and phased-array antenna applications, and analog front-end readout integrated circuits for lidar applications.